Journal of *Marine Science and Engineering*

MDPI

Article

Settling Velocity of Microplastics Exposed to Wave Action

Annalisa De Leo [1,*], Laura Cutroneo [2], Damien Sous [3,4] and Alessandro Stocchino [5]

[1] DICCA, Università degli Studi di Genova, via Montallegro 1, 16145 Genova, Italy
[2] DISTAV, Università degli Studi di Genova, Corso Europa 26, 16132 Genova, Italy; laura.cutroneo@dipteris.unige.it
[3] Université de Toulon, Aix Marseille Université, CNRS, IRD, Mediterranean Institute of Oceanography (MIO), 83130 La Garde, France; damien.sous@mio.osupytheas.fr
[4] Université de Pau et des Pays de l'Adour-E2S UPPA, SIAME-MIRA, 64012 Anglet, France
[5] Department of Civil and Environmental Engineering, Hong Kong Polytechnic University, Hung Hom, Kowloon, Hong Kong, China; alessandro.stocchino@polyu.edu.hk
* Correspondence: annalisa.deleo@edu.unige.it; Tel.: +39-010-33-56576

Abstract: Microplastic (MP) debris is recognized to be one of the most serious threats to marine environments. They are found in all seas and oceanic basins worldwide, even in the most remote areas. This is further proof that the transport of MPs is very efficient. In the present study, we focus our attention on MPs' transport owing to the Stokes drift generated by sea waves. Recent studies have shown that the interaction between heavy particles and Stokes drift leads to unexpected phenomena mostly related to inertial effects. We perform a series of laboratory experiments with the aim to directly measure MPs' trajectories under different wave conditions. The main objective is to quantify the inertial effect and, ultimately, suggest a new analytical formulation for the net settling velocity. The latter formula might be implemented in a larger scale transport model in order to account for inertial effects in a simplified approach.

Keywords: microplastic transport; Stokes drift; inertial particles; settling velocity

Citation: De Leo, A.; Cutroneo, L.; Sous, D.; Stocchino, A. Settling Velocity of Microplastics Exposed to Wave Action. *J. Mar. Sci. Eng.* **2021**, *9*, 142. https://doi.org/10.3390/jmse9020142

Academic Editor: Michele Arienzo
Received: 7 January 2021
Accepted: 26 January 2021
Published: 29 January 2021

1. Introduction

The marine environment is continuously and increasingly threatened by pollution derived from anthropogenic activities, through the uncontrolled release of waste and dangerous substances transported by winds and rivers from land to sea. Among these, the presence of plastics, of different sizes, is now recognized as one of the main threats to the whole environment [1]. Its global production has increased significantly over the past few decades, reaching more than 348 million tonnes in 2017; see for example the Annual Report issued by the Association PlasticsEurope [2]. A widely accepted definition of Microplastics (MPs) requires plastic particles to be smaller than 5 mm in size [3]. However, a clear and accepted terminology and classification is still under discussion [4], as well as a standardization of the plastic collection and analysis methods [5]. Besides the dimensions, it is important to note that MPs' mass densities are generally close to that of water, but may be either positively or negatively buoyant [3,6]. The mass density depends primarily on the plastic composition, with a wide range of values (e.g., high density polyethylene, 930–970 kg·m^{-3}, polypropylene, 850–920 kg·m^{-3}, polyvinyl chloride, 1300–1450 kg·m^{-3}), which can be further modified in the marine environment by degradation or colonization of biofouling and weathering processes [7–9]. These aspects play a fundamental role on the fate of plastic debris in the environment, primarily influencing the settling velocity of the plastic particles. Several studies have been dedicated to the accurate estimation of the settling velocities depending on the main physical properties of the particles, namely size, shape, and density [10–12].

A great effort has been devoted in these last ten years to quantifying the plastics' (micro and macro) abundance in different compartments (surface water, water column, and

sediment) of open seas and other delicate environments (coastal areas, estuaries, and rivers); see among others Hidalgo et al. (2012) [3], Law (2017) [13], and Rezaina et al. (2018) [14] for comprehensive reviews. The main outcome of these studies was that plastics in different forms (floating debris, microplastic pieces, and plastic fibers) are found in every sea basin around the world, with higher concentrations occurring in intense human activity areas. A recent field campaign found a non-negligible plastic content even in the most remote sea basins [15,16]. This demonstrates that plastic debris transport can be extremely efficient and that the prediction of the plastics' fate is of paramount importance. Plastics' dispersion is driven by a number of physical processes, acting over a wide range of scales; it is worth mentioning the predominant effects of oceanic and coastal currents and wind and sea wave transport through the Stokes drift. Most efforts to numerically model MPs' transport in the ocean or coastal areas treat the particles as neutrally buoyant tracers [17–19]. Other models include effects related to wind-induced mixing and a superimposed constant settling velocity [8,20–26]. Overall, most of the classical approaches in MP dispersion substantially disregard inertial effects owing to buoyancy and drag. Recent contributions have been devoted to filling in this gap in understanding the role of the inertial character of heavy particles, using more refined models to describe the particle trajectories. More specifically, the particle model of Maxey and Riley (1983) [27] has been employed in theoretical and numerical models to study the interactions among negatively buoyant spherical [28,29] and non-spherical [30] particles and the sea wave Stokes drift. Additional insight into the inertial effects has been provided by recent experimental laboratory studies of MP dispersion in the nearshore [31].

In the present study, we aim to experimentally investigate the inertial Stokes drift depending on several controlling parameters, i.e., wave and particle characteristics. The results will be used to validate previous models and, ultimately, to suggest a new analytical formulation of the net settling velocity to describe MPs' transport in wave-exposed environments.

2. Materials and Methods

2.1. Experimental Setup

The experiments were performed in the MIO/SEATECHwave flume at SEATECH Engineering School, University of Toulon. The flume is 13 m long, 30 cm wide, and 50 cm deep. The net length of the flume that can be used for experimental measurements is about 10 m. The flume is equipped with a piston wave-maker with a pneumatic actuator, remotely controlled using a digital signal acquisition/generation system. The flume side walls are made of thick glass panels, allowing for direct visualization and video recordings. For the present experiments, the water depth was kept constant and equal to 26.5 cm. A dissipative sloping beach was installed at the end of the flume to minimize the effects of wave reflection. Regular waves were imposed with variable periods and amplitudes. During each experiment, the generated wave field was monitored using three wave gauges (sampling frequency of 200 Hz), placed in the center line of the flume at 1, 2.22, and 2.64 m downstream of the wave maker. The wave gauge data were analyzed in order to compute the wave characteristics (period and amplitude) through peak analysis and to quantify the reflection at the dissipative beach following the three gauges method [32,33]. A schematic overview of the experimental setup is shown in Figure 1.

The recovered wave data for the five wave cases are summarized in Table 1. The dimensionless parameter H/gT^2 is employed to synthetically describe a sea state; see [34]. It can also be viewed as a measure of wave steepness: for a given wave period T, higher values of H/gT^2 correspond to higher and steeper waves, since the wave period is related to the wavelength through the dispersion relationship. The set of waves generated in the present experimental campaign was such that the wave parameter H/gT^2 was monotonically increasing moving from the first wave condition (W1) to the last one (W4). Overall, the experimental values of H/gT^2 were in a realistic range, and they can well represent typical sea state conditions of several sea basins [29]. All wave conditions fell

in the intermediate depth regime except for W1, which corresponded to shallow water conditions. The reflection coefficient ranged between 0.16 and 0.23, which means that the reflection effect was quite small.

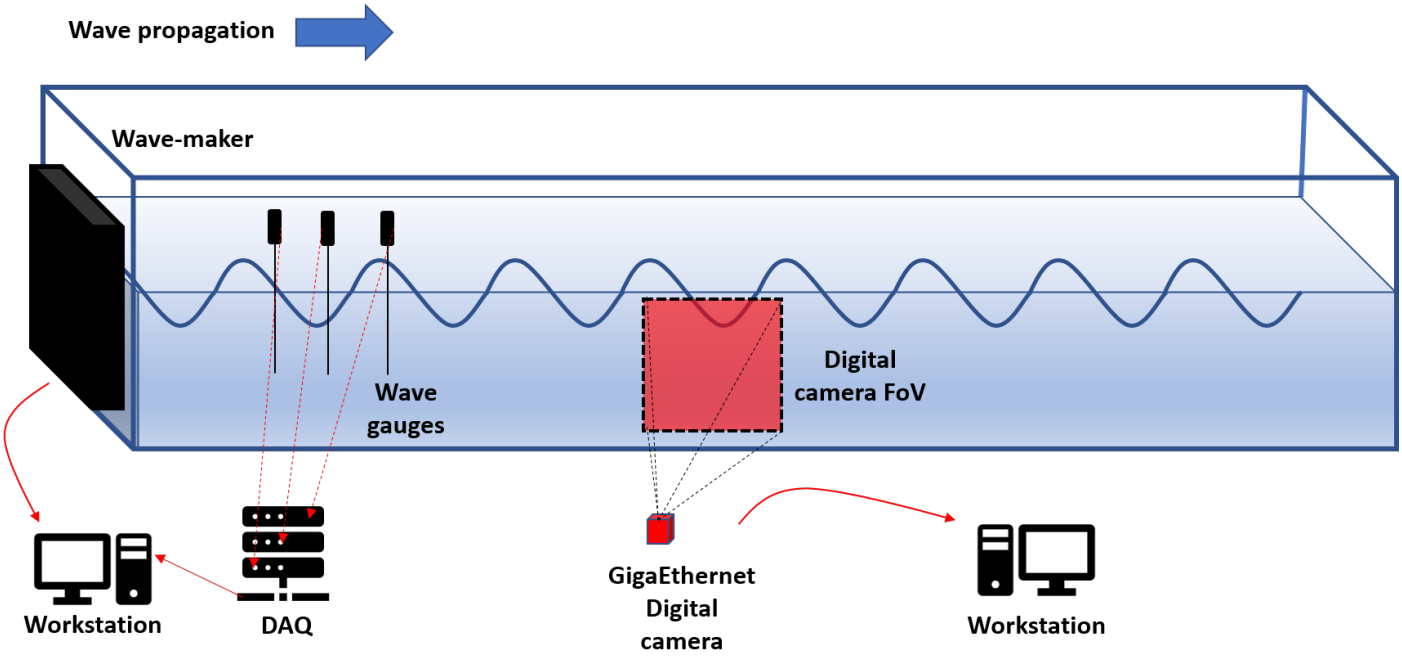

Figure 1. Schematic view of the experimental setup.

Table 1. Measured wave conditions. The reflection coefficient R was evaluated following [32]. The last column refers to the experiment number. 3.

Wave Condition	H (m)	T (s)	R	H/gT^2	Exp.
W1	0.031	0.85	0.23	0.0044	7–12
W2	0.041	0.85	0.16	0.0058	13–18
W3	0.077	0.85	0.17	0.0108	19–24
W4	0.033	0.5	0.18	0.0134	25–30

2.2. Particles

The selected PMMA (polymethyl methacrylate) particles had a fixed density $\rho_p = 1190$ kg·m^{-3} and different diameters d_p ranging from 150 and 640 µm. The PMMA particles were initially sold as a mixture with a poorly sorted grain size distribution. The particles were, therefore, previously sieved to obtain six grain classes with narrow size distributions; see Figure 2.

The particle diameters were evaluated using microscope imaging analyzed with a specific software (open-source software ImageJ, imagej.nih.gov). Size statistics for the six selected classes are reported in Table 2. A particle diameter distribution was defined starting from a list of diameter sizes within the selected sieve. Than, they were ranged and normalized by the total amount of the sampled diameters. The d_x diameter is the diameter at which x% of particles are finer and (100-x)% of particles are coarser. The resulting size distributions were narrow enough to consider the d_{50} diameter as representative of the PMMA particle diameter, simply named d_p in the following. Plastic particles were

characterized in terms of their added mass, represented by the dimensionless parameter β, and their drag response through the Stokes response time τ, defined as:

$$\beta = \frac{3\rho_f}{\rho_f + 2\rho_p} \quad (1)$$

$$\tau = \frac{d_p^2}{12\beta\nu} \quad (2)$$

where ρ_f is the density of the fluid, water in the present case, and ν its dynamic viscosity. For the present experiments, the added mass parameter β kept a constant value equal to 0.8876. Note that the well-known Stokes number can be readily evaluated as $S_t = \omega\tau$, where $\omega = 2\pi/T$ is the angular frequency of the waves.

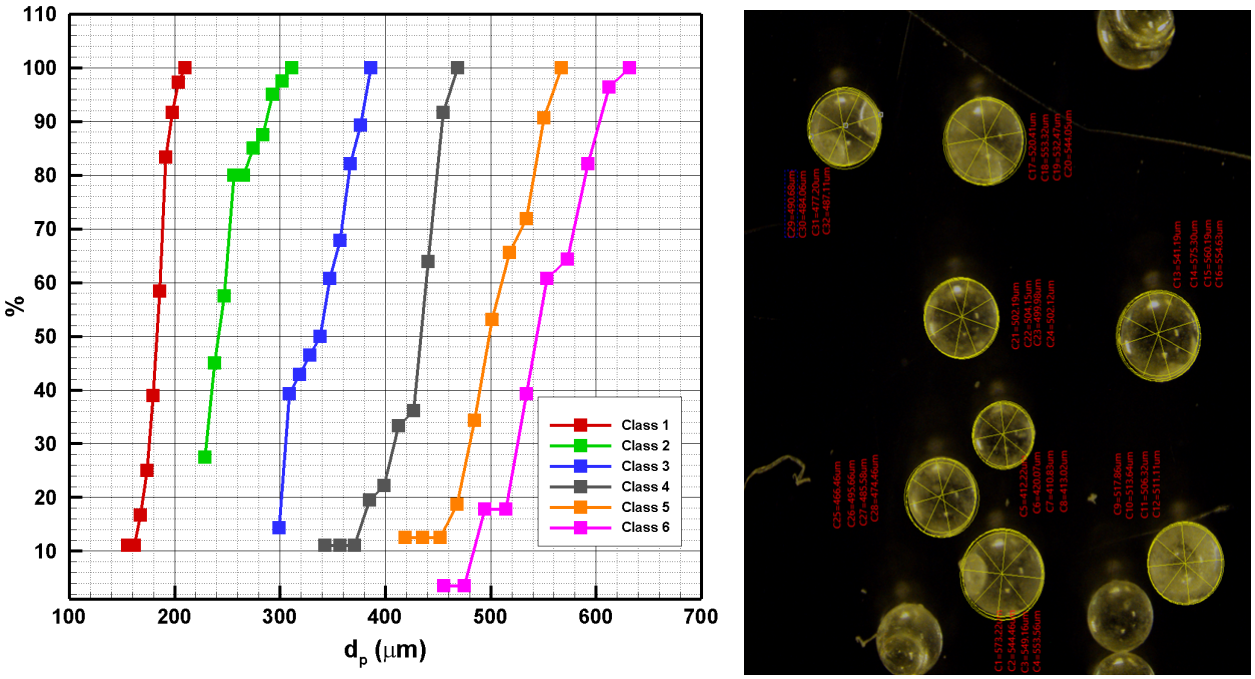

Figure 2. Left panel: Particle diameter distributions for the six selected classes. Right panel: Example of microscope images with the particle diameter measurements.

Table 2. Main parameters for the six selected classes of PMMA particles.

Class	d_{16} (μm)	d_{50} (μm)	d_{84} (μm)
1	512	543	574
2	468	498	528
3	417	433	451
4	307	338	368
5	217	241	267
6	173	183	193

2.3. Test Cases

A total of 30 experiments were performed. The main experimental parameters (wave and particles) are reported in Table 3. Four different wave conditions were tested by varying the period and amplitude; see Table 1 for further details. For each wave condition, all particle classes were released and tested. Experiments 1 to 6 (not reported in Table 3) were dedicated to the experimental protocol testing and therefore not considered for the physical analysis. For each experiment, the particles of a specific diameter class were released manually at the free surface, a few millimeters below it to avoid surface tension

effects. The release was repeated several times during a single acquisition in order to increase the number of measured trajectories.

Table 3. Experimental wave and particle parameters.

Exp.	d_p (μm)	T (s)	H (m)	τ	S_t
007	543	0.85	0.031	0.029	0.214
008	498	0.85	0.031	0.024	0.177
009	433	0.85	0.031	0.017	0.127
010	338	0.85	0.031	0.011	0.079
011	241	0.85	0.031	0.006	0.044
012	183	0.85	0.031	0.003	0.023
013	543	0.85	0.041	0.029	0.214
014	498	0.85	0.041	0.024	0.177
015	433	0.85	0.041	0.017	0.127
016	338	0.85	0.041	0.011	0.079
017	241	0.85	0.041	0.006	0.044
018	183	0.85	0.041	0.003	0.023
019	543	0.85	0.077	0.029	0.214
020	498	0.85	0.077	0.024	0.177
021	433	0.85	0.077	0.017	0.127
022	338	0.85	0.077	0.011	0.079
023	241	0.85	0.077	0.006	0.044
024	183	0.85	0.077	0.003	0.023
025	543	0.5	0.033	0.029	0.363
026	498	0.5	0.033	0.024	0.302
027	433	0.5	0.033	0.017	0.216
028	338	0.5	0.033	0.011	0.135
029	241	0.5	0.033	0.006	0.075
030	183	0.5	0.033	0.003	0.040

2.4. Settling Trajectory Measurements

The present measurement strategy was specifically designed to track the trajectories of settling particles under the influence of waves. The particle motion was recorded by a high-definition GigaEthernet digital camera (Teledyne Dalsa Genie Nano C2450) with a 25mm lens. The camera CCD is a $2/3^{''}$ format with a resolution of 2448 $\times$ 2048 pixel. The frame rate was adjusted for each experiment, ranging between 20 and 25 fps. The camera optical axis was kept orthogonal to the flume glass wall. The Field of View (FoV) was about 22 $\times$ 28 cm, allowing visualizing the entire flow depth and the horizontal movements of the settling particles. The illumination of the FoV was obtained using four 500 W white light halogen lamps, complemented, in some cases, with a 200 mW solid state laser.

A single acquisition typically lasted between 100 and 200 s, producing between 2500 and 4000 images depending on the frame rate. A systematic background removal was applied on each image to eliminate spurious reflections and regions with non-uniform illumination. The resulting images were then binarized by applying a proper threshold based on the image intensity to ease subsequent analysis.

The processed images were analyzed using the tracking software MotionStudio^{TM} (Integrated Design Tool, Inc, Pasadena (CA), 91103-3070, USA). The tracking procedure started manually by indicating the features that the software shall track in the image sequence and setting a small area around the interested particle, namely an Interrogation Window (IW). The tracking algorithm is based on a cross-correlation of the IW between successive pairs. The above procedure was applied many times on the same image sequence in order to obtain a statistically significant set of particle trajectories. In general, for each experiment, we obtained a variable number of single particle trajectories between 30 and 60 depending on the quality of the images: diameters lower than 300 μm were generally more difficult to track, owing to both the size and a lack of proper illumination. In fact, based on the field of view of the images and the resolution of the digital camera, a single pixel

represents about 100 μm. Particles with diameters smaller than 300 μm became comparable with the pixel size, and then, their tracking was impossible. In order to overcome this limitation, both increasing the digital camera resolution or decreasing the field of view would enable the tracking of this class of particles. The present method is similar to the particle image velocimetry technique used in a recent study [12].

3. Results and Discussion

3.1. Measured Particle Trajectories

Figure 3 shows four examples of measured trajectories for Experiments 8, 12, 13, and 17. Experiments 8 and 12 were performed with wave conditions W1 with two different particle size classes, namely with $d_p = 498$ μm and $d_p = 183$ μm, respectively. Similarly, Experiments 13 and 17 were performed with the wave conditions W2, characterized by the same period as W1, but a larger wave height, in which another set of particle diameter was considered ($d_p = 543$ μm and $d_p = 241$ μm, respectively).

It is worth mentioning that for a neutrally buoyant particle, i.e., $\beta = 1$, the expected trajectory driven by the wave Stokes drift would be an open spiral with no net transport in the vertical position after a single wave period [35]. As soon as a particle had a density difference with the fluid, i.e., $\beta < 1$, the particle trajectory substantially deviated from the $\beta = 1$ case. Figure 3 shows that in each case, the particles tended to settle following a trajectory that resembled a spiral, which, as time passed, tended to unroll itself. This effect was stronger for larger diameters (Figure 3, Panels a and c). As soon as the settling particle no longer felt the presence of the Stokes drift, the trajectories would be identical to that expected for pure settling in still fluid, i.e., a straight vertical line. For the smallest diameter (Figure 3, Panels b and d), the spiral-like trajectory was better preserved during the particle settling, reaching a depth comparable to the total flow depth. In all cases, in the limit for long times, the trajectories would be straight vertical lines.

The behavior described above for the experiments reported in Figure 3 can be considered typical of all experiments performed during the present study. Similar behaviors have been presented in recent theoretical and numerical studies [28–30]. The inertial character of the particles is the main reason to this difference with respect to the Stokes drift trajectories for a fluid particle. The effect of wave height H translates into a more intense Stokes drift that is felt at greater depths. In fact, the intensity of the Stokes drift can be estimated from bulk wave parameters [36], and it is proportional to the wave height and the angular frequency. In particular, it depends quadratically on the wave height and linearly on the wave angular frequency. Increasing the wave height H, or equivalently the wave parameter H/gT^2 for a given wave period, will lead the particle trajectories to manifest the rolling character for longer times, experiencing a more intense Stokes drift.

Finally, Figure 4 shows the time evolution of the particle velocities for two typical experiments, namely Experiment 8 and 12. The interaction between the inertial effects and the Stokes drift leads to an evolution of the velocity components that is periodic over time, which oscillates with a period equal to the wave period and a decreasing amplitude. Note that the longitudinal velocity component v_x oscillates around a zero value, which will be reached at a long time. In fact, as time tends to infinity, the particle reaches a depth where the Stokes drift is no longer acting, and thus, the particle, at that stage, would only settle with a zero horizontal velocity component similarly as still fluid settling. On the other hand, at the long time limit, the vertical velocity reaches an asymptotic value equal to the still fluid settling velocity for that specific particle. Experiments 8 and 12 were carried out with the same wave conditions, and the observed difference highlights the influence of the Stokes number.

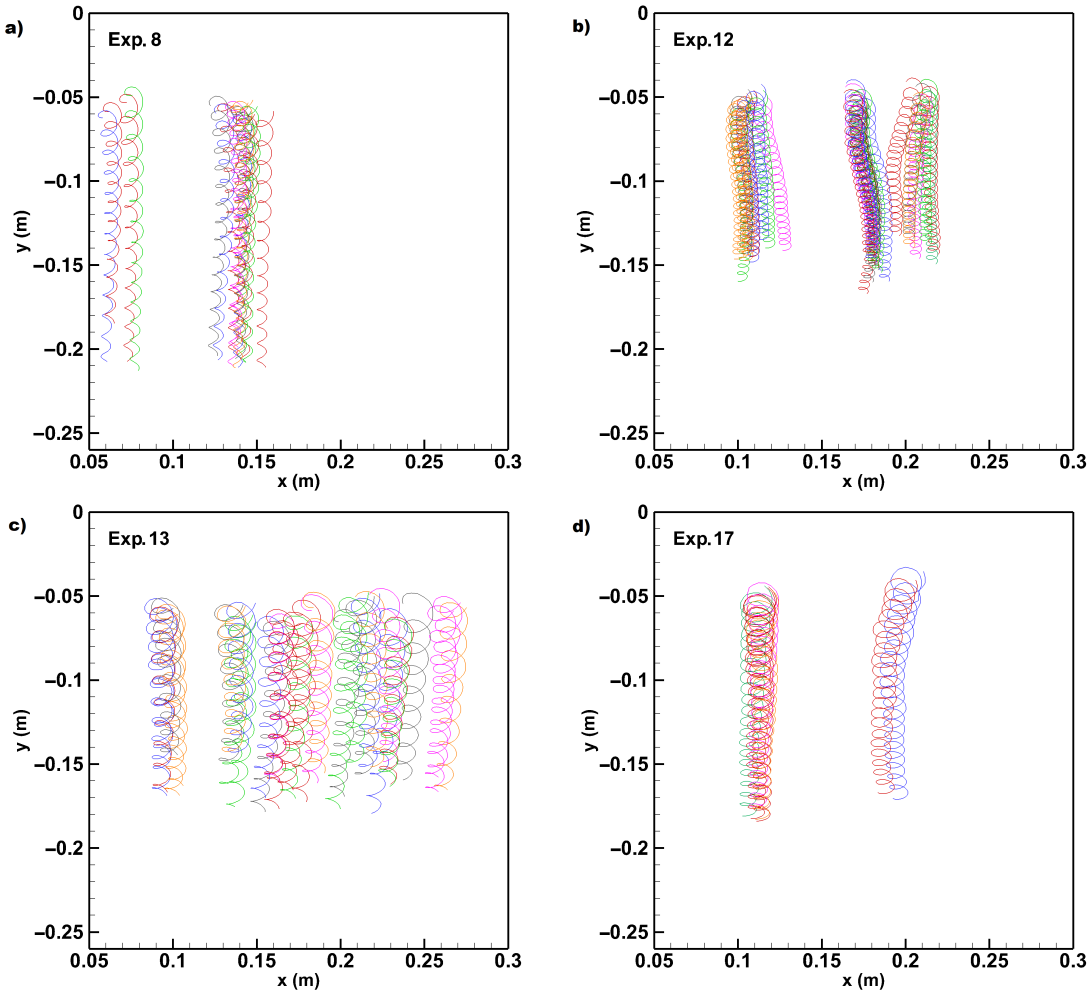

Figure 3. Examples of measured trajectories for Experiments (**a**) 8, (**b**) 12, (**c**) 13, and (**d**) 17.

3.2. the Role of the Inertial Stokes Drift on the Net Settling Velocity

The estimation of the settling velocity of plastic particles in a wave-exposed marine environment is of paramount importance for the prediction of plastics' dispersion and abundance. The settling velocity enters as a physical parameter in several modeling approaches employed to produce large-scale predictions of the distribution of microplastics in several sea basins [21,24,25,37**?**]. So far, the inclusion of the particle settling velocity has been done tentatively to consider the inertial character of the plastics. In fact, the motion of a spherical inertial particle could be described by the following set of equations:

$$\frac{d\mathbf{x}(t)}{dt} = \mathbf{V}(t) \tag{3}$$

$$\frac{d\mathbf{V}(t)}{dt} = \frac{\mathbf{u}(\mathbf{x},t) - \mathbf{V}(t)}{\tau} + (1-\beta)\mathbf{g} + \beta\frac{d\mathbf{u}(\mathbf{x},t)}{dt} \tag{4}$$

where $\mathbf{V}(t)$ is the Lagrangian particle velocity at the position $\mathbf{x}(t)$ and $\mathbf{u}(\mathbf{x},t)$ the flow field acting on the particle. This model is obtained by the original set of equations of Maxey and Riley (1983) [27] for a spherical particle, neglecting the Faxen and Basset terms from the original equations. The solution of the above system provides an accurate description of the physics of the present problem [28–30] and in more complex oceanographic flows [38]. Large-scale models for plastic transport, based on Lagrangian and Eulerian equations, often implement the settling velocity as a steady solution of Equation (4) by equating the drag force term (second term on the right-hand side) and the gravitational force term

(third term on the right-hand side), disregarding the effect of time dependency of the latter system. Thus, the quest for a good empirical estimator of the settling velocity has inspired numerous studies dedicated to plastic particles [10–12]. The dominant approach has been to test the applicability of well-known settling formulas to plastic particles. For instance, Khatmullina and Isachenko (2017) [11] used several empirical models developed in other contexts such as settling of natural sediment grains [39,40] or formulas developed for non-spherical particles [41]. A recent study followed a similar approach on a wider range of particle parameters [12]. However, it should be emphasized that all tested formulas have been developed in pure settling in still fluids, which represents a limiting case since the transport in marine environments is dominated by an intense dynamics and, in particular, by sea waves. Aiming to provide further insight on the settling velocity in wave-exposed environments, the present measurements of particles trajectories obtained for a fairly wide range of particle and wave parameters are further processed to provide estimates of the net settling velocity. In the wave context, this latter is defined as the effective settling velocity generated by the effect of the inertial Stoke drift as a result of the interaction between drag forces, described by τ and the gravity force, described by β and wave transport. The analysis is performed on the time evolution of the vertical position $y(t)$ extracted from the full trajectories; see Figure 5 for examples, where Panels (a) and (c) show the measured trajectories for Experiments 8 and 12. The net settling velocity is then directly estimated from the slope of the linear fitting of the $y(t)$ signal (Figure 5b,d).

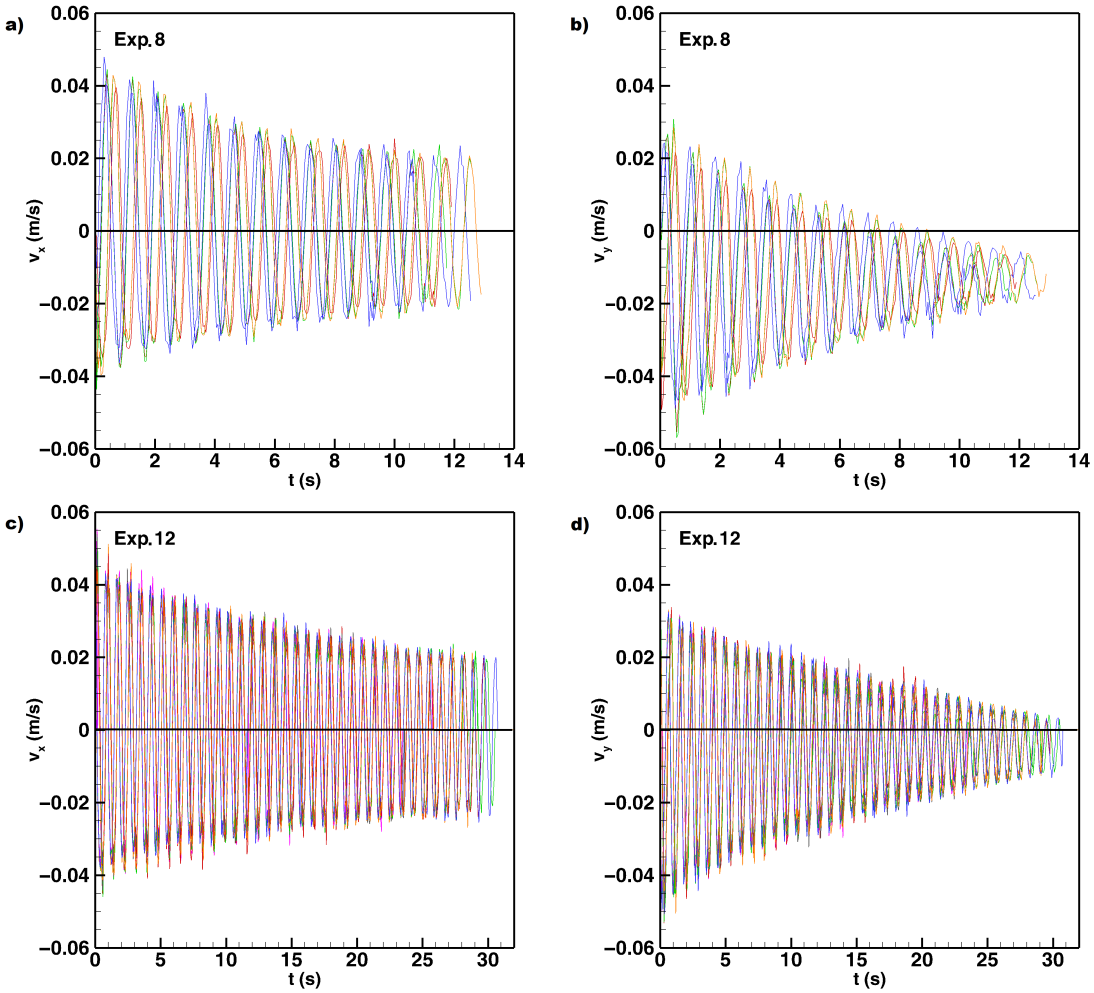

Figure 4. Time evolution of the particle velocities: (**a**) Experiment 8 x-component, (**b**) Experiment 8 y-component, (**c**) Experiment 12 x-component, and (**d**) Experiment 12 y-component.

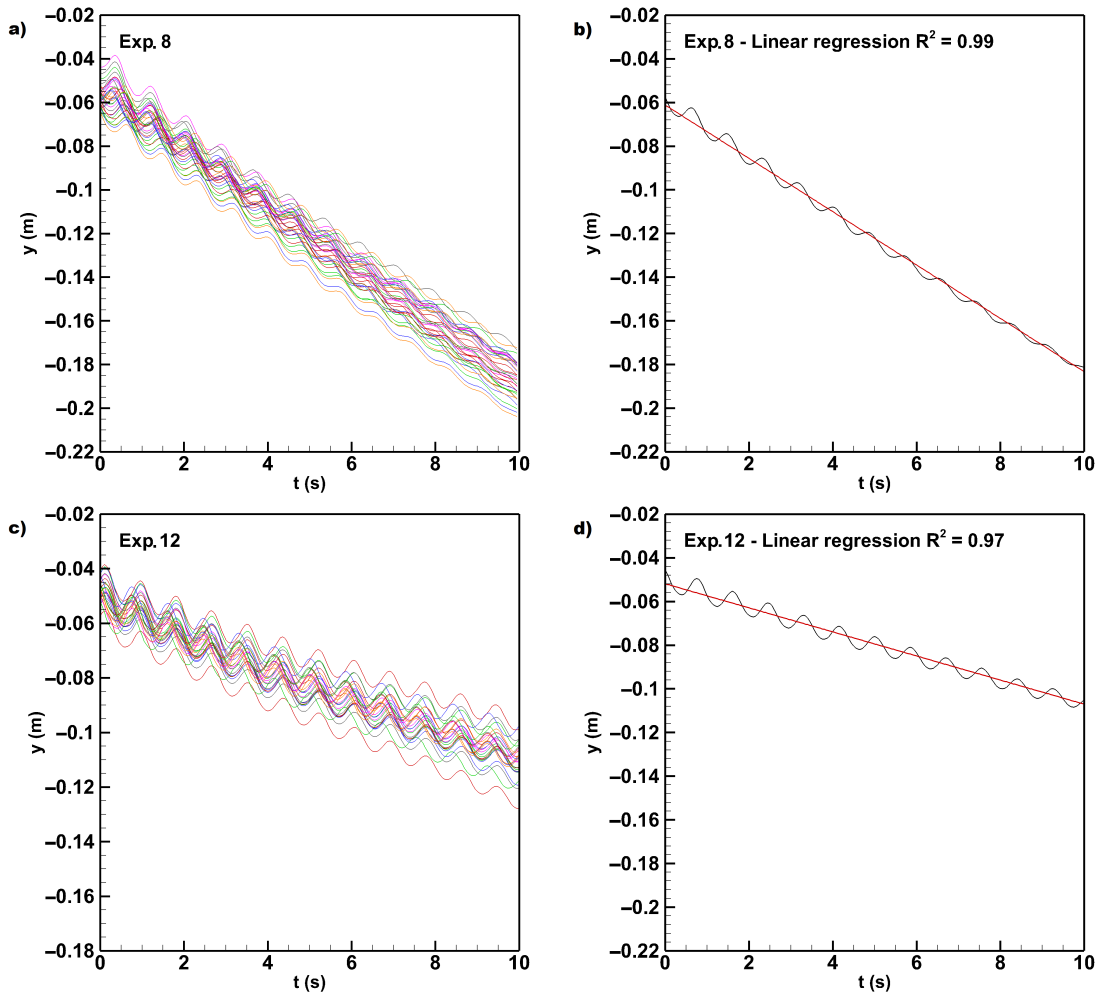

Figure 5. Time evolution of the vertical displacements for Experiments (**a**) 8 and (**c**) 12. In Panels (**b**) and (**d**) are shown the linear regressions of a single track, respectively for Experiments 8 and 12.

The linear regression filters out the $y(t)$ periodic components with an R-squared (R^2) ranging between 0.7 and 0.99, indicating the reliability of the linear model. Figure 6 displays the measured net settling velocity in non-dimensional form $w_s^* = w_s^3/g'\nu$ versus the squared particle Reynolds number $R_p^2 = g' d_p^3/\nu^2$; where $g' = g(\rho_p - \rho_f)/\rho_f$ is the reduced gravity acceleration and ν is the kinematic fluid viscosity (see [11] for a similar scaling). Note that Figure 6 is in log-log coordinates. In the same plot, the theoretical prediction of settling velocity provided by the Dietrich's formula [39] is also reported for comparison, as it is commonly used to describe plastics' settling velocities. In particular, we calculated the settling velocity by means of the latter formula for each diameter d_p. As expected, the dimensionless settling velocity increases for a higher particle Reynolds number. Moreover, it is worth noting that for a fixed value of the particle Reynolds number, R_p, the net settling velocity increases monotonically with the wave parameter, H/gT^2. This observation suggests that increasing the wave amplitude for a given wave period, and therefore increasing the intensity of the Stokes drift, produces an increment of the net settling velocity. Moreover, the effect of the inertial Stokes drift is stronger for small R_p, leading to a greater difference with respect to the still water settling velocity. On the contrary, as R_p increases, the particle dynamics tends to a pure settling, collapsing with the settling velocity prediction obtained by the Dietrich formula.

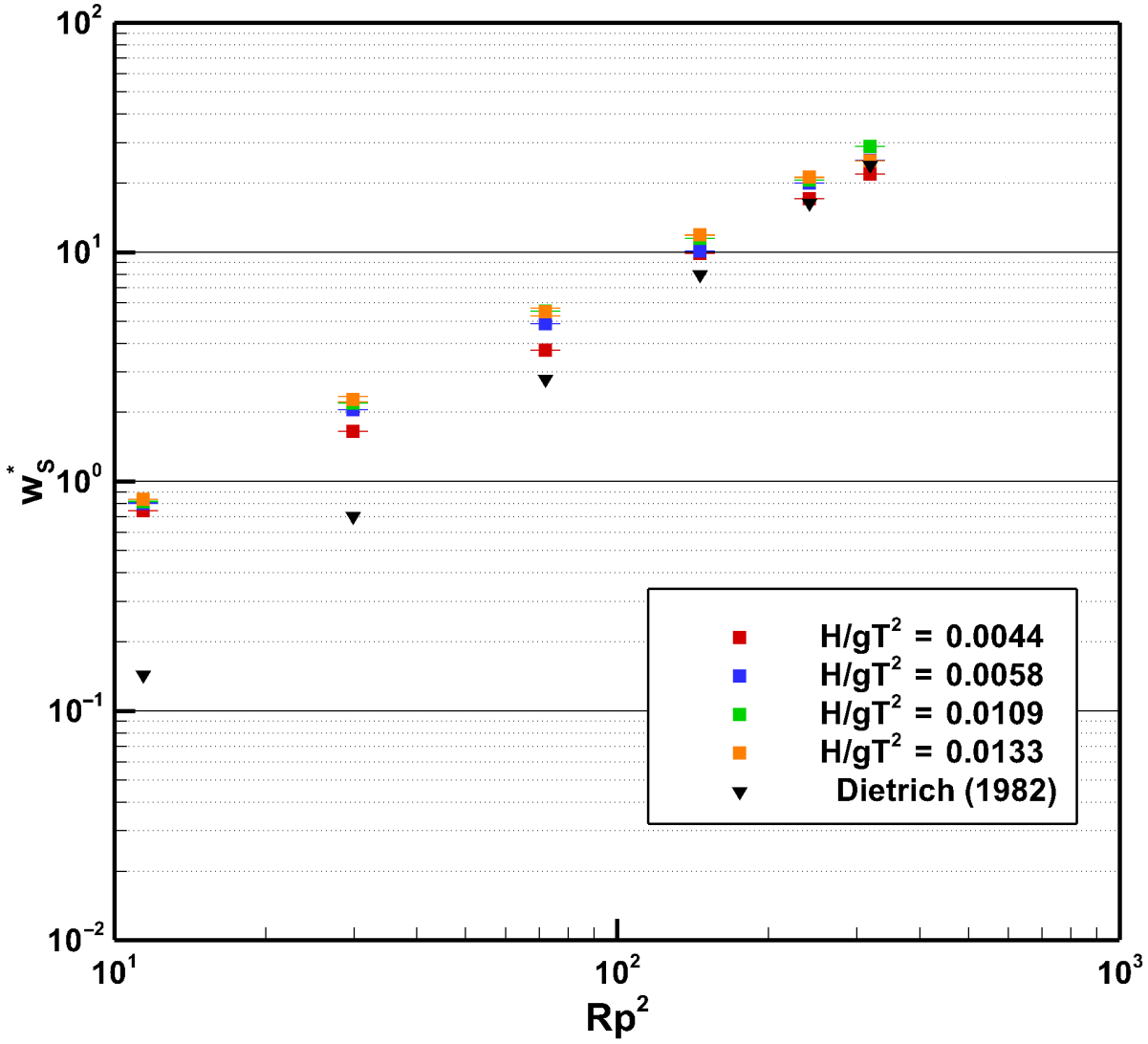

Figure 6. Non-dimensional net settling velocity w_s^* as a function of the squared particle Reynolds number.

To better compare the present results in a wave-exposed context with the traditional pure settling velocity formulas, Figure 7 depicts the measured net settling velocity w_s^m for all experiments against the theoretical estimate with the Dietrich formula. The solid line indicates perfect agreement, whereas the black and blue dashed-dotted lines indicate the ±20% and ±50% thresholds, respectively. The results clearly indicate that the overall effect of the inertial Stokes drift is to increase the settling velocity compared to the case of pure settling in still fluid. Most of the experimental measurements fall inside the region of ±50%. On the contrary, the smallest diameters, which correspond to the lowest velocities, show greater differences, indicating that they are more sensitive to the effect of the Stokes drift. Santamaria et al. (2013) [28] showed that inertial particles tend to increase the settling velocity under regular waves and only asymptotically tend to the Stokes terminal velocity. Similar results have been obtained numerically with a more refined wave model by Stocchino et al. (2019) [29]. The numerical prediction reported in [29] is fairly consistent with the present results. For particle diameters in a range between 300 and 500 µm, the increase with respect to the pure settling velocity was estimated by the numerical simulation of the order of 20% for the smallest diameter and about 6% for the largest. In the present laboratory experiments, for the same diameter, the increase is of the order of 15–20% and 5–9%, respectively.

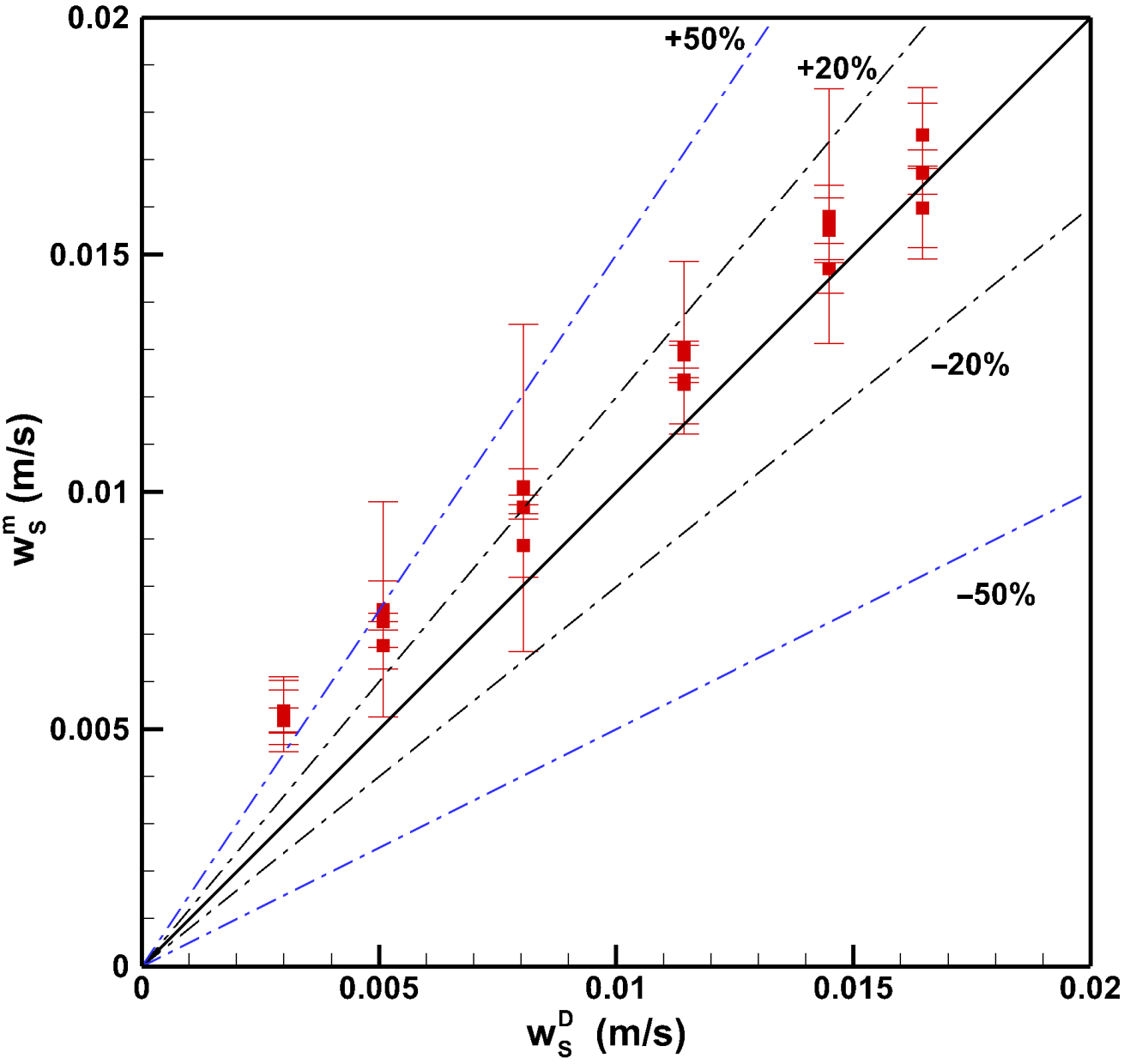

Figure 7. Comparison between the measured net settling velocity against the theoretical settling velocity as in Dietrich (1982). Rectangles are the mean of the measured settling velocities with their standard deviation; the black solid line is the plane bisector, indicating perfect agreement, whereas the black and the blue dotted-dashed lines represent the ±20% and ±50% confidence intervals, respectively.

3.3. A New Formulation of the Settling Velocity

We aim to present an analytic interpretation of the measured settling velocity. As already mentioned, settling velocity formulas are often implemented in numerical models at the regional or oceanographic scale, and the common choice is to use the expressions that have been tested in still water [11]; the effect of waves is added using Stokes drift classical formulations. The present laboratory experiments demonstrated that the interaction of inertial effects and sea wave Lagrangian transport produces a more complex settling dynamics of the plastic particles. Aiming to provide a simple and operable approach, we suggest a new formulation of the settling velocity that empirically takes into account the inertial Stokes drift. The proposed formulation should satisfy the limit when no wave field is acting, i.e., $H/gT^2 = 0$, and thus, the settling occurs as in still water. In this limit case,

we decided to describe the settling velocity by the well established Dietrich formula, which we recall here for the sake of clarity. The Dietriech settling velocity w_s^D can be estimated as:

$$w_s^D = \sqrt{\frac{g'}{g} d_P R_f} \tag{5}$$

where R_f is:

$$\begin{aligned} R_f = \exp\Big\{ & -b_0 + b_1 \ln(R_P) - b_2[\ln(R_P)]^2 \\ & -b_3[\ln(R_P)]^3 + b_4[\ln(R_P)]^4 \Big\} \end{aligned} \tag{6}$$

in which the coefficients b_0–b_4 are fitted on experimental data and assume the values: 2.89139, 0.95296, 0.05683, 0.00289, and 0.00024. Note that the original values of the coefficient were changed in order to implement the natural logarithm instead of the base-10 logarithm, as in the original form [39].

Starting from the measured non-dimensional settling velocity defined as the ratio between the experimental net settling velocity w_s^m and the velocity w_s^D provided by Equation (5), we intend to represent the dependency on the main parameters, namely the particle Reynolds number R_p and the wave parameter H/gT^2, using the following formulation:

$$\frac{w_s^m}{w_s^D} = 1 + a R_P^b \left(\frac{H}{gT^2} \right)^c \tag{7}$$

where the coefficients a, b, and c are evaluated as the best fit on the experimental data. A non- linear surface fitting is applied, based on an iterative trust-region-reflective least squares algorithm [42–44]. Applying this procedure on the experimental data, using Equation (7), leads to the values of the parameters $a = 97$, $b = 8/5$, and $c = 3/5$. The fitted surface is shown in Figure 8 together with the experimental data. The goodness of the non-linear fit is quantified using several statistical metrics, in particular the Sum of Squares Due to Error (SSE), R-squared (R^2), and the Root Mean Squared Error ($RMSE$). For the present database, we obtained $SSE = 0.1798$, $R^2 = 0.9108$, and $RMSE = 0.0787$. The small values of SSE and $RMSE$ indicate that the model used to describe the dataset through Equation (7) shows a small random error component, implying that the model is robust in terms of prediction in the parameter space. Moreover, the high value of the R^2 indicates that the suggested formula describe about 91% of the total variation in the data about the average. The overall goodness of fit values confirm that the proposed model is statistically robust in representing the experimental observations and gives confidence for a more general application on the estimation of the settling velocity of microplastic particles exposed to wave action.

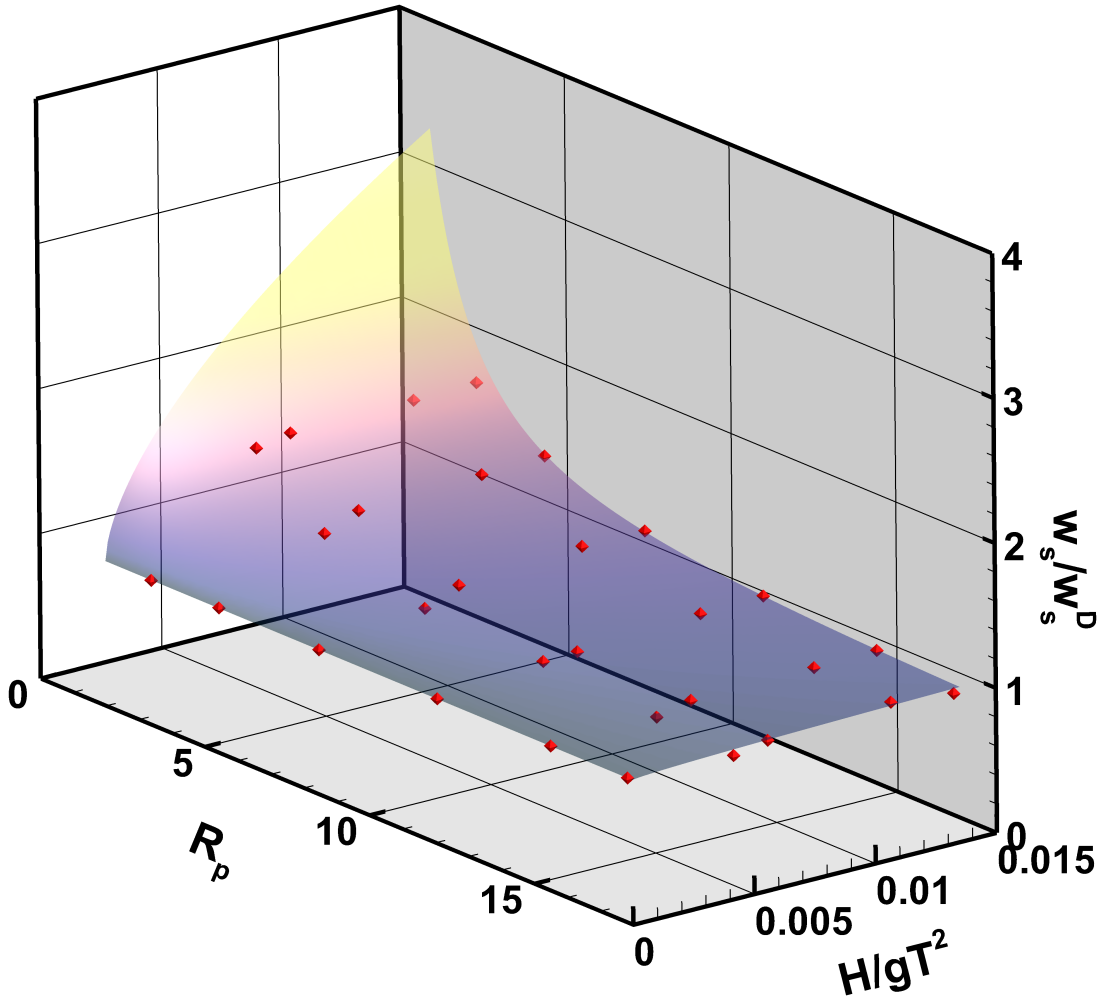

Figure 8. Reconstructed surface using Equation (7) in the parameter space (R_p, H/gT^2) versus the experimental net settling velocity.

3.4. Scaling Argument and Applicability of the Results

The present results were obtained using a laboratory wave flume as described in the Methods Section. It is worth discussing the limitation and applicability of the measurements, comparing the setup and controlling the parameters with the actual field observations. Scale reproduction of free surface flows, such as waves, is typically achieved through a partial similarity of the Froude number, defined as the ratio between inertial and gravitational forces, $Fr = U/\sqrt{gL}$, where L and U are typical scales for the length and velocity. As a consequence of this choice, some of the parameters used for the present analysis require a proper scaling in order to extend the results to real-world conditions. The Froude similitude implies that a geometrical reduction scale λ should be associated with a time scale reduction as $\lambda^{1/2}$, which also ensures the preservation of the wave parameter H/gT^2 between the model and the real sea waves. The present laboratory waves in the range of $H/gT^2 = 0.004 - 0.013$ are representative of realistic sea state conditions; see [29] for comparison. The main particle parameters that have been used in the present study are the Stokes number S_t and the particle Reynolds number R_p. In the Froude similitude, both are scaled as a typical Reynolds number and, thus, as $\lambda^{3/2}$. The range of the parameters investigated at the laboratory scale is $S_t = 0.023 - 0.363$ and $R_P = 3.39 - 17.9$ for a fixed

value of the particle density that corresponds to $\beta = 0.8876$. The direct comparison of such ranges at the field scale is not straightforward due to the fact that, despite the great amount of literature reporting field observations of plastic debris in different sea/ocean basins and different compartments (water surface, water column, and sediment), it remains difficult to have comprehensive information on the particle size and density. Hidalgo et al. (2012) [3] presented an interesting review based on 68 studies trying to summarize the range of particle debris in terms of sizes and densities. However, it is interesting to note that heavy particles have been often collected during sediment sampling with quite a wide range of sizes [45,46]. We based our estimate of the Stokes number and particle Reynolds number on a recent work [6] where a helpful statistical interpretation of the data derived from eleven published studies was presented. In particular, a multidimensional probability density function (pdf) involving the size, density, and shapes of the debris was proposed. In particular, the distribution of plastic density is well fit by a normal-inverse Gaussian distribution with a central value of around 1000 kg·m^{-3} and a marked positive skewness with non-negligible probability values up to 1600 kg·m^{-3} [6]. From this analysis, about 45% of the observed plastic debris had a density in a range between 960 and 1580 kg·m^{-3}, not considering the chemical and weathering process that tend to increase plastic density; see Table S3 of [6]. Based on the analysis of [6], in particular the data of their Figures S1 and S4 and Table S3, we used a range of particle sizes $d_p = 100 - 4000\mu$m and density $\rho_P = 1030 - 1300$ kg·m^{-3}. Using a range of the wave parameter similar to the one used for the present experiments, the Stokes number and the particle Reynolds number obtained are $S_t = 0.002 - 11$ and $R_P = 0.5 - 430$ for a range of added mass parameters β between 0.848 and 0.997. The experimental ranges of S_t and R_P are therefore fully included in the ranges expected at field scale. We could conclude that the present formulation for a net settling velocity of heavy particles well represents the realistic conditions of the transport of plastic particles by sea waves, for quite a wide range of realistic plastic characteristics. We acknowledges the limitation of the present study in considering only spherical particles and the fact that our wave flume does not allow for the generation of sea waves in deep water conditions. The former issue will deserve further investigations based on the present study. The latter, however, it is not considered as a main factor in the dynamics of negatively buoyant particles.

4. Conclusions

The present study reports a laboratory investigation of the interaction between inertial heavy particles, as a realistic model for MP particles and the Stokes drift generated by sea waves. A series of experiments was performed in a wave flume to cover a range of particle and wave parameters. The regular waves fall in intermediate and shallow depth conditions, with dimensionless sea state parameter H/gT^2 ranging from 0.0044 to 0.0134. Fixed-density, but variably-sized PMMA particles were employed to cover a range of Stokes number between 0.023 and 0.363, for a fixed value added mass parameter of 0.8876. The measurements reproduced typical behaviors predicted by previous theoretical and numerical models [28,29], confirming the validity of the model approaches. In addition, the results have shown a clear dependence of the net settling velocity, not only on the particle characteristics, described by the particle Reynolds number, but also on the wave characteristics, through the sea state parameter H/gT^2. The inertial effects lead to a remarkable increase of the particle settling velocity with respect to the one predicted by standard formulas validated in still fluids [10,11,39]. The increased settling velocity is more evident as the particle Reynolds number decreases, highlighting the tendency for larger particles to match more rapidly the still fluid settling velocity than smaller ones. The present results have been interpreted in terms of a modified version of the standard Dietrich formula [39] allowing accounting for wave dependency. The implementation of the latter formula into a regional or larger scale transport model should improve the prediction of the fate of heavy MPs, including a simplified description of inertial effects. Future research will be dedicated to understanding the role of the particle shapes and

their importance on the net settling velocity, as well as a wider range of the added mass parameter. This aspect might be further complicated by biofouling [7–9], which is able to change the overall density and, then, the inertial properties of MPs.

Author Contributions: A.D.L. performed the experiments, analyzed the results, and wrote the first draft of the paper; L.C. analyzed the results and revised the paper; D.S. designed the experiments, analyzed the results, and revised the paper; A.S. designed the experiments, analyzed the results, and revised the paper. All authors read and agreed to the published version of the manuscript.

Funding: This research was financially supported by the Project Splash!, Stop alle Plastiche in H20!, funded by the Interreg Italia-Francia Marittimo Program.

Institutional Review Board Statement: Not applicable.

Informed Consent Statement: Not applicable.

Data Availability Statement: The data presented in this study are available on request from the corresponding author.

Acknowledgments: The authors would like to thank Aimed Ajroud for his help during the laboratory experiments.

Conflicts of Interest: The authors declare no conflict of interest. The funders had no role in the design of the study; in the collection, analyses, or interpretation of data; in the writing of the manuscript; nor in the decision to publish the results.

References

1. Villarrubia-Gómez, P.; Cornell, S.E.; Fabres, J. Marine plastic pollution as a planetary boundary threat–The drifting piece in the sustainability puzzle. *Mar. Policy* **2018**, *96*, 213–220.
2. PlasticsEurope. *Annual Report 2018 "Plastics—the Facts 2018. An Analysis of European Latest Plastics Production, Demand and Waste Data"*; Technical Report, PlasticsEurope: Brussels, Belgium, 2018.
3. Hidalgo-Ruz, V.; Gutow, L.; Thompson, R.C.; Thiel, M. Microplastics in the marine environment: a review of the methods used for identification and quantification. *Environ. Sci. Technol.* **2012**, *46*, 3060–3075.
4. Hartmann, N.B.; Huffer, T.; Thompson, R.C.; Hassellov, M.; Verschoor, A.; Daugaard, A.E.; Rist, S.; Karlsson, T.; Brennholt, N.; Cole, M. Are we speaking the same language? Recommendations for a definition and categorization framework for plastic debris. *Environ. Sci. Technol.* **2019**, *53*, 1039–1047.
5. Cutroneo, L.; Reboa, A.; Besio, G.; Borgogno, F.; Canesi, L.; Canuto, S.; Dara, M.; Enrile, F.; Forioso, I.; Greco, G.; Lenoble, V.; Malatesta, A.; Mounier, S.; Petrillo, M.; Rovetta, R.; Stocchino, A.; Tesan, Javier Vagge, G.; Capello, M. Microplastics in seawater: sampling strategies, laboratory methodologies, and identification techniques applied to port environment. *Environ. Sci. Pollut. Res.* **2020**, 27(9), 8938–8952
6. Kooi, M.; Koelmans, A.A. Simplifying microplastic via continuous probability distributions for size, shape, and density. *Environ. Sci. Technol. Lett.* **2019**, *6*, 551–557.
7. Kaiser, D.; Kowalski, N.; Waniek, J.J. Effects of biofouling on the sinking behavior of microplastics. *Environ. Res. Lett.* **2017**, *12*, 124003.
8. Kooi, M.; Nes, E.H.v.; Scheffer, M.; Koelmans, A.A. Ups and downs in the ocean: effects of biofouling on vertical transport of microplastics. *Environ. Sci. Technol.* **2017**, *51*, 7963–7971.
9. Porter, A.; Lyons, B.P.; Galloway, T.S.; Lewis, C. Role of marine snows in microplastic fate and bioavailability. *Environ. Sci. Technol.* **2018**, *52*, 7111–7119.
10. Chubarenko, I.; Bagaev, A.; Zobkov, M.; Esiukova, E. On some physical and dynamical properties of microplastic particles in marine environment. *Mar. Pollut. Bull.* **2016**, *108*, 105–112.
11. Khatmullina, L.; Isachenko, I. Settling velocity of microplastic particles of regular shapes. *Mar. Pollut. Bull.* **2017**, *114*, 871–880.
12. Waldschlager, K.; Schuttrumpf, H. Effects of particle properties on the settling and rise velocities of microplastics in freshwater under laboratory conditions. *Environ. Sci. Technol.* **2019**, *53*, 1958–1966.
13. Law, K.L. Plastics in the marine environment. *Annu. Rev. Mar. Sci.* **2017**, *9*, 205–229.
14. Rezania, S.; Park, J.; Din, M.F.M.; Taib, S.M.; Talaiekhozani, A.; Yadav, K.K.; Kamyab, H. Microplastics pollution in different aquatic environments and biota: A review of recent studies. *Mar. Pollut. Bull.* **2018**, *133*, 191–208.
15. Bergmann, M.; Wirzberger, V.; Krumpen, T.; Lorenz, C.; Primpke, S.; Tekman, M.B.; Gerdts, G. High quantities of microplastic in Arctic deep-sea sediments from the HAUSGARTEN observatory. *Environ. Sci. Technol.* **2017**, *51*, 11000–11010.
16. Suaria, G.; Perold, V.; Lee, J.R.; Lebouard, F.; Aliani, S.; Ryan, P.G. Floating macro-and microplastics around the Southern Ocean: Results from the Antarctic Circumnavigation Expedition. *Environ. Int.* **2020**, *136*, 105494.
17. Maximenko, N.; Hafner, J.; Niiler, P. Pathways of marine debris derived from trajectories of Lagrangian drifters. *Mar. Pollut. Bull.* **2012**, *65*, 51–62.

18. Ballent, A.; Pando, S.; Purser, A.; Juliano, M.; Thomsen, L. Modelled transport of benthic marine microplastic pollution in the Nazaré Canyon. *Biogeosciences* **2013**, *10*, 7957.
19. Zambianchi, E.; Trani, M.; Falco, P. Lagrangian transport of marine litter in the Mediterranean Sea. *Front. Environ. Sci.* **2017**, *5*, 5.
20. Kukulka, T.; Proskurowski, G.; Morét-Ferguson, S.; Meyer, D.; Law, K. The effect of wind mixing on the vertical distribution of buoyant plastic debris. *Geophys. Res. Lett.* **2012**, *39*.
21. Isobe, A.; Kubo, K.; Tamura, Y.; Nakashima, E.; Fujii, N.Selective transport of microplastics and mesoplastics by drifting in coastal waters. *Mar. Pollut. Bull.* **2014**, *89*, 324–330.
22. Kukulka, T.; Brunner, K. Passive buoyant tracers in the ocean surface boundary layer: 1. Influence of equilibrium wind-waves on vertical distributions. *J. Geophys. Res. Ocean.* **2015**, *120*, 3837–3858.
23. Brunner, K.; Kukulka, T.; Proskurowski, G.; Law, K. Passive buoyant tracers in the ocean surface boundary layer: 2. Observations and simulations of microplastic marine debris. *J. Geophys. Res. Ocean.* **2015**, *120*, 7559–7573.
24. Zhang, H. Transport of microplastics in coastal seas. *Estuarine, Coast. Shelf Sci.* **2017**, *199*, 74–86.
25. Liubartseva, S.; Coppini, G.; Lecci, R.; Creti, S. Regional approach to modeling the transport of floating plastic debris in the Adriatic Sea. *Mar. Pollut. Bull.* **2016**, *103*, 115–127.
26. Liubartseva, S.; Coppini, G.; Lecci, R.; Clementi, E.Tracking plastics in the Mediterranean: 2D Lagrangian model. *Mar. Pollut. Bull.* **2018**, *129*, 151–162.
27. Maxey, M.; Riley, J. Equation of motion for a small rigid sphere in a nonuniform flow. *Phys. Fluids* **1983**, *26*, 883–889.
28. Santamaria, F.; Boffetta, G.; Afonso, M.M.; Mazzino, A.; Onorato, M.; Pugliese, D. Stokes drift for inertial particles transported by water waves. *EPL (Europhys. Lett.)* **2013**, *102*, 14003.
29. Stocchino, A.; De Leo, F.; Besio, G. Sea Waves Transport of Inertial Micro-Plastics: Mathematical Model and Applications. *J. Mar. Sci. Eng.* **2019**, *7*, 467.
30. DiBenedetto, M.H.; Ouellette, N.T.; Koseff, J.R. Transport of anisotropic particles under waves. *J. Fluid Mech.* **2018**, *837*, 320–340.
31. Forsberg, P.L.; Sous, D.; Stocchino, A.; Chemin, R. Behaviour of plastic litter in nearshore waters: first insights from wind and wave laboratory experiments. *Mar. Pollut. Bull.* **2020**, *153*, 111023.
32. Drevard, D.; Rey, V.; Fraunié, P. Partially standing wave measurement in the presence of steady current by use of coincident velocity and/or pressure data. *Coast. Eng.* **2009**, *56*, 992–1001.
33. Rey, V.; Capobianco, R.; Dulou, C. Wave scattering by a submerged plate in presence of a steady uniform current. *Coast. Eng.* **2002**, *47*, 27–34.
34. LeMéhauté, B. *An introduction to Hydrodynamics and Water Waves*; Environmental Science Servies Administration: Berlin, Germany, 1969, Volume 52.
35. Stokes, G.G. *On the Effect of the Internal Friction of Fluids on the Motion of Pendulums*; Pitt Press Cambridge: Cambridge, UK, 1851, Volume 9
36. Kumar, N.; Cahl, D.L.; Crosby, S.C.; Voulgaris, G. Bulk versus spectral wave parameters: Implications on stokes drift estimates, regional wave modeling, and HF radars applications. *J. Phys. Oceanogr.* **2017**, *47*, 1413–1431.
37. Jalón-Rojas, I.; Xiao-Hua, W.; Fredj, E. On the importance of a three-dimensional approach for modelling the transport of neustic microplastics. *Ocean. Sci.* **2019**, *15*, 717–724.
38. Beron-Vera, F.J.; Olascoaga, M.J.; Miron, P. Building a Maxey–Riley framework for surface ocean inertial particle dynamics. *Phys. Fluids* **2019**, *31*, 096602.
39. Dietrich, W.E. Settling velocity of natural particles. *Water Resour. Res.* **1982**, *18*, 1615–1626.
40. Zhiyao, S.; Tingting, W.; Fumin, X.; Ruijie, L. A simple formula for predicting settling velocity of sediment particles. *Water Sci. Eng.* **2008**, *1*, 37–43.
41. Clift, R.; Grace, J.; Weber, M. Nonspherical rigid particles at higher Reynolds numbers. *Bubbles Drops Part.* **1978**, pp. 142–168.
42. Moré, J.J.; Sorensen, D.C. Computing a trust region step. *SIAM J. Sci. Stat. Comput.* **1983**, *4*, 553–572.
43. Steihaug, T. The conjugate gradient method and trust regions in large scale optimization. *SIAM J. Numer. Anal.* **1983**, *20*, 626–637.
44. Coleman, T.F.; Li, Y. An interior trust region approach for nonlinear minimization subject to bounds. *SIAM J. Optim.* **1996**, *6*, 418–445.
45. McDermid, K.J.; McMullen, T.L. Quantitative analysis of small-plastic debris on beaches in the Hawaiian archipelago. *Mar. Pollut. Bull.* **2004**, *48*, 790–794.
46. Morét-Ferguson, S.; Law, K.L.; Proskurowski, G.; Murphy, E.K.; Peacock, E.E.; Reddy, C.M. The size, mass, and composition of plastic debris in the western North Atlantic Ocean. *Mar. Pollut. Bull.* **2010**, *60*, 1873–1878.